Preparation, Structure, and Surface Chemistry of Ni-Au Single Atom Alloys

Zhi-Tao Wang[a,c], *Matthew T. Darby*[b], *Andrew J. Therrien*[a], *Mostafa El-Soda*[a], *Angelos Michaelides*[d], *Michail Stamatakis*[b], *E. Charles H. Sykes*[a*]

[a]Department of Chemistry, Tufts University, Medford, Massachusetts 02155-581, USA

[b]Thomas Young Centre and Department of Chemical Engineering, University College London, Roberts Building, Torrington Place, London, WC1E 7JE, UK

[c]Department of Chemistry and Chemical Biology, Harvard University, Cambridge, Massachusetts 02138, USA

[d]Thomas Young Centre, London Centre for Nanotechnology and Department of Physics and Astronomy, University College London, 17-19 Gordon Street, London, WC1H 0AH, UK

* To whom correspondence should be addressed to charles.sykes@tufts.edu (617 627 3773)

Abstract

Ni/Au is an alloy combination that while, immiscible in the bulk, exhibits a rich array of surface geometries that may offer improved catalytic properties. It has been demonstrated that the addition of small amounts of Au to Ni tempers its reactivity and reduces coking during the steam reforming of methane. Herein, we report the first successful preparation of dilute Ni-Au alloys (up to 0.04 ML) in which small amounts of Ni are deposited on, and alloyed into, Au(111) using physical vapor deposition. We find that the surface structure can be tuned during deposition *via* control of the substrate temperature. By adjusting the surface temperature in the 300 K to 650 K range, we are able to produce first Ni islands, then mixtures of Ni islands and Ni-Au surface alloys, and finally, when above 550 K, predominantly island-free Ni-Au single atom alloys (SAAs). Low-Temperature Scanning Tunneling Microscopy (STM) combined with Density Functional Theory calculations confirm that the Ni-Au SAAs formed at high temperature correspond to Ni atoms exchanged with surface Au atoms. Ni-Au SAAs form preferentially at the elbow regions of the Au(111) herringbone reconstruction, but at high coverage also appear over the whole surface. To investigate the adsorption properties of Ni-Au SAAs, we studied the adsorption and desorption of CO using STM which allowed us to determine at which atomic sites the CO adsorbs on these heterogeneous alloys. We find that small amounts of Ni in the form of single atoms increases the reactivity of the substrate by creating single Ni sites in the Au surface to which CO binds significantly more strongly than Au. These results serve as a guide in the design of surface architectures that combine Au's weak binding and selective chemistry with localized, strong binding Ni atom sites that serve to increase reactivity.

1. Introduction

Due to weak substrate-adsorbate interactions, Au-based catalysts exhibit high selectivity for a range of hydrogenation and oxidation reactions under low-temperature conditions.[1-9] Such catalysts however tend to have low activity due to gold's full d-band.[10] It has been demonstrated that activity can be improved by using Au nanoparticles that alter the electronic properties and reduce surface atom coordination.[1] An alternative chemical strategy however is to alloy a more reactive transition metal into the Au surface. Ni may be an ideal candidate as its negative mixing enthalpy in the surface region of Au and high surface free energy drives both lateral surface dispersion and diffusion into the bulk.[11-14] The metal's demonstrated catalytic utility – Ni is one of the most widely used industrial catalysts – makes it further appealing to be investigated at the ultra-dilute limit. Ni supported on alumina or magnesium oxide, for example, is the current standard catalyst in steam reforming of methane.[15-18] This major industrial process produces synthesis gas, which in turn fuels other large-scale reactions including Fischer-Tropsch synthesis and methanol synthesis.[16-17] Single Atom Alloys (SAAs), isolated reactive metal adatoms dispersed in the surface layer of a more inert host metal, have generated significant interest as catalysts in recent years. Numerous studies so far have demonstrated the capability of SAAs to catalyze hydrogenations,[19-22] dehydrogenations,[23] oxidations,[24-25] hydrogenolysis[26] and coupling reactions.[27] While Cu is a catalytically inert metal for example, Pd-Cu SAAs can enable the facile activation of H_2, spillover of hydrogen atoms onto Cu and subsequent hydrogenation of styrene and acetylene.[28] A recent study revealed a direct link between single crystal and nanoparticle catalysts of Pt-Cu SAAs which show high activity and selectivity for butadiene hydrogenation to butenes, demonstrating transferability from the model study to the catalytic reaction under practical conditions.[29] Using the opposite approach, Besenbacher *et al*. found that

adding small amounts of Au to Ni(111) tempered surface reactivity and reduced catalyst coking and transferred this result to a real catalyst.[30-31] In the current work, we have alloyed small amounts of Ni into Au(111) to produce SAAs and demonstrated their potential for increasing the binding strength of adsorbates using CO as a probe molecule.

As the thermodynamically-favored facet of Au nanoparticles, Au(111) is the most commonly studied model surface. Although the Ni-Au system has been studied for several decades, previous work focused on the epitaxy and properties of Ni islands Au(111) rather than Ni-Au SAAs.[11-12, 32-33] Meyer *et al.* showed that the Ni adatoms initially exchange with Au atoms at edge dislocations of the Au (22×√3) herringbone reconstruction.[32] Those surface-layer atoms then become nucleation sites for subsequent Ni atoms to form islands.[32] To form SAAs in that system, the surface concentration of Ni must be reduced. That concentration reduction was initially hypothesized to be possible through the equilibrium diffusion of Ni into the bulk at elevated temperatures. Cullen *et al.* and Trant *et al.* however showed that thermal annealing of Ni islands only resulted in changes in the distribution of island sizes and/or level of Ni aggregation in sub-surface layers instead of the dispersion of Ni in the surface layer of Au.[11-12] Kinetic limitations are therefore necessary to prevent the formation of islands at the nucleation sites. We propose that elevating the substrate temperature during the deposition process, rather than *ex post*, will give Ni atoms access to sufficient thermal energy to avoid trapping and accumulation at their nucleation sites. However, Cullen and First attempted to deposit Ni on Au(111) at 450 K and only observed large, disordered islands rather than Ni-Au SAAs.[11] In the work presented herein we re-examined this surface alloy and observed atomic-sized depressions in scanning tunneling microscopy (STM) images in the herringbone reconstruction of Au(111), and identified them using Density Functional Theory (DFT) calculations as substitutional Ni

atoms in and under the Au surface.[32, 34] We employ physical vapor deposition and STM to explore in detail the effect of temperature on the growth of Ni on Au(111). In particular, we identify the conditions necessary to prepare varying concentrations of Ni-Au SAAs without the formation of any Ni islands. The structure of Ni-Au SAAs is examined in depth by combining STM data with DFT calculations. We then use carbon monoxide (CO) adsorption to investigate preferential binding sites on the Ni-Au(111) alloys.

2. Experimental section

All experiments were conducted in an ultra-high vacuum (UHV) low temperature (LT) STM chamber (Omicron Nanotechnology). Au(111) substrates on mica were cleaned under UHV by multiple alternating short Ar^+ sputtering (1 keV/15 μA) and thermal anneal (1000 K) cycles. We found that it was necessary to use a Au film on mica rather than a Au single crystal because after Ni deposition it is not possible to completely remove Ni from the Au crystal and the relatively cheap contaminated Au on mica substrates could be thrown away. Ni was evaporated from a flux-monitored Omicron electron beam evaporator at seven substrate temperatures (300 K, 350 K, 450 K, 500 K, 550 K, 600 K, and 650 K). A constant Ni flux of 0.02 monolayers (ML) min^{-1} was used for all depositions, with the deposition time used to control the total amount of Ni deposited. In this paper the monolayer refers to the density of Au atoms on the unreconstructed Au(111) (1 ML=1.387×10^{15} atoms/cm^2). CO adsorption was performed in the STM chamber with background dosing at 5 K. Exposures are quoted in langmuirs (L, 1 L=1×10^{-6} Torr·s). STM images were recorded at 5 K or 80 K with a background pressure below 1×10^{-11} mbar.

Periodic density functional theory calculations were performed using the Vienna *ab* initio Simulation Package (VASP) version 5.3.3.[35-36] A plane-wave kinetic energy cutoff of 400 eV is

used for the valence electron expansion and the core electrons are accounted for using projector augmented wave potentials. Methfessel-Paxton smearing is used with a smearing width of 0.1 eV. The exchange-correlation functional used is the non-local OptB86b-vdW[37-38] functional, which is a revised version of the van der Waals density functional of Dion *et al*.[39] Lattice constants for bulk face-centered cubic (fcc) Au and Ni are optimized to be 4.137 Å and 3.494 Å respectively, with the former used in Ni-Au alloy calculations. We use a 3 × 3 × 5 slab unit cell whereby the topmost four layers are allowed to fully relax while the bottommost layer is fixed by the OptB86b-vdW lattice constant. Our calculations on Au(111) and alloys with Ni use slabs of unreconstructed fcc Au only, we do not account for the herringbone reconstruction. Slabs are separated from periodic images in the *z*-direction with a vacuum of ~20 Å. The Brillouin zone is sampled using a gamma-centered 13 × 13 × 1 Monkhorst-Pack *k*-point grid within the 3 × 3 unit cell. Ionic relaxation is performed on all structures until the Hellmann-Feynmann forces acting on all free atoms are below 0.01 $eV \cdot Å^{-1}$ whilst ensuring that the electronic minimization remains self-consistent at each ionic step up to a tolerance of 10^{-7} eV. All calculations are spin-polarized.

3. Results and Discussion

Figure 1a shows a typical Au(111) surface with the characteristic herringbone pattern, referred to as a (22×√3) reconstruction.[40-41] Briefly, to increase the average coordination of surface Au atoms, extra atoms pack into the surface layer at equilibrium, producing a lattice mismatch between the surface and bulk atomic spacings. This mismatch appears in STM images as bright pairs of lines, called soliton walls, seen in Figure 1. The soliton walls lie in three equivalent orientations 120° apart, reflecting the three-fold symmetry of the hexagonal lattice, and hence reduce surface strain isotropically. Soliton walls are separated by alternating regions of hexagonally close-packed (hcp) and fcc domains, reflecting the atomic registry with the

underlying layers. When two soliton walls intersect they form edge dislocations at the 'elbows.' Under-coordinated surface atoms at these edge dislocations tend to make the elbows the most reactive regions of the Au(111)-(22×√3) surface. After Ni deposition at 350 K, Meyer et al. observed the formation of depressions at the elbows that they attributed to substitution of Ni into the surface.[32] The STM image shown in Figure 1b of Au(111) after deposition of ~0.004 ML Ni at 300 K reveals atomic sized depressions at the elbows (see white arrows) and bright features that have been previously identified as Ni islands at elbows (see blue arrows).[11-12] Despite our slightly lower surface temperature during alloying, we also attribute the depressions in Figure 1b to Ni-Au exchange given the high Ni surface free energy relative to Au. These depressions act as nucleation sites during alloying, trapping Ni atoms to form islands at elbows and occasionally on soliton walls (see blue arrows). STM images of Au(111) after deposition of ~0.004 ML Ni at 350 K and 450 K are displayed in Figures 1c and 1d. At these higher temperatures, a higher concentration of Ni depressions is observed. Close inspection however reveals that most of these features are apparently larger than the depressions showed in Figure 1b and include small clusters in the centers (see yellow arrows), which we interpret to be small Ni clusters at the nucleation stage.[32] At higher temperature, Ni has higher diffusion rates both into the bulk and across the surface, increasing the probability of exchanging with surface Au atoms but also reducing the probability of trapping and accumulation at nucleation sites.

When the substrate temperature during deposition is raised above 500 K (Figure 1e-h), the islands disappear while depressions become more abundant (see green arrows). With the same appearance as those in Figure 1b and as observed by Meyer *et al*., these depressions can be interpreted as single-atom Ni substitutions, which is supported by DFT STM image simulations discussed later in this paper. Even above 450 K however, the concentration of depressions on the

surface is significantly lower than the total concentration of deposited Ni atoms. This result implies a significant diffusion of Ni into the bulk, in good agreement with Trant *et al*.'s finding that monolayer Ni segregates into the subsurface layers of Au(111) when annealed above 460 K.[12]

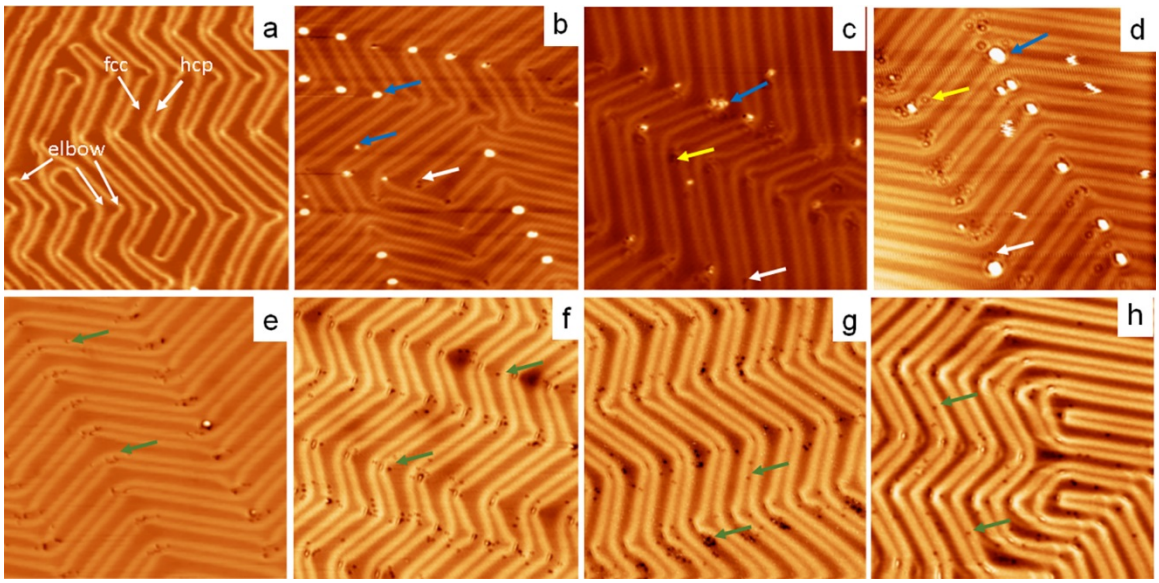

Figure 1. (a) STM image of a clean Au(111) surface with the fcc, hcp and elbow regions of the reconstruction highlighted with arrows. (b-h) STM images of Au(111) after deposition of ~0.004 ML of Ni at 300 K (b), 350 K (c), 450 K (d), 500 K (e), 550 K (f), 600 K (g), and 650 K (h). In b-h, the yellow, blue, white and green arrows highlight, respectively, Ni clusters, Ni islands, Ni-Au SAAs formed at low temperature, and SAAs formed at high temperature. Imaging conditions: 50 mV-200 mV, 1.0 nA-2.5 nA, 80 K. Image size: 50 nm×50 nm.

STM images in Figure 2a-c depict Au(111) surfaces after deposition of ~0.02 ML Ni at 300 K, 350 K, and 450 K. On surfaces alloyed at 300 K and 350 K, Ni islands appear at almost every elbow, in agreement with previous reports.[11] With a 450 K deposition temperature however, some elbows are bare. Island formation is therefore dependent on both Ni coverage and

deposition temperature. Increasing Ni deposition increases the size of islands but not their concentration. We attribute this phenomenon to either the Ostwald ripening effect or more likely the fact that islands initially formed act as nucleation points for subsequently deposited Ni atoms.[42] Comparing the surfaces formed at 450 K and 500 K, this effect becomes clear, with much fewer and much larger islands, at the higher temperature (Figure 2d). Cullen and First similarly observed large islands after annealing Ni on Au(111) at 500 K. They however identified them as Au islands owing to their observation of a Au herringbone reconstruction on top of the islands.[11] We observe no such long-range ordering on our islands and thus propose they contain both Ni and Au, as suggested in previous reports.[11-12]

Ni/Au(111) surfaces formed by deposition of ~0.02 ML Ni at 500 K, 550 K and 600 K (Figure 2d-f) display similar morphologies of depressions. These high temperatures produce a high concentration of depressions in both the elbows and the (22x√3) surface, with a significant change in quantity and distribution of depressions when compared to the lower temperature depositions (Figure 2b and c). At 650 K (Figure 2g), a significant drop in the concentration of depressions is observed, suggesting that more of the Ni atoms are diffusing into the bulk than at 550 K and 600 K. Again we see that not only the amount of deposited Ni but also the deposition temperature can be used to control the surface concentration of single-atom Ni substitutions. As we observed at the lower Ni depositions, no islands form when deposition is performed above 550 K (Figure 2e-g). Figure 2h displays a typical STM image of the Au(111) surface after deposition of ~0.16 ML Ni at 550 K, an 8-fold increase in coverage over Figure 2e. While the concentration of depressions increases commensurately, the surface remains free of islands.

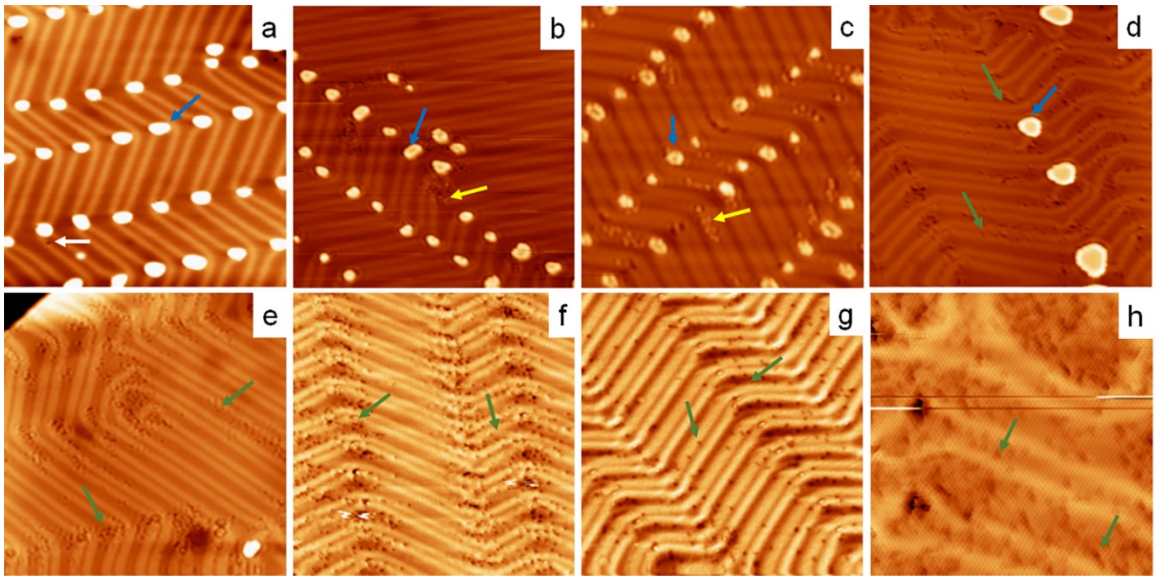

Figure 2. STM images of Au(111) after deposition of ~0.02 ML of Ni at 300 K (a), 350 K (b), 450 K (c), 500 K (d), 550 K (e), 600 K (f) and 650 K (g), and after deposition of ~0.16 ML of Ni at 550 K (h). The yellow, blue, white and green arrows highlight Ni clusters, Ni islands, Ni-Au SAAs formed at low temperature and SAAs formed at high temperature, respectively. Imaging conditions: 50 mV-200 mV, 1.0 nA-2.5 nA, 80 K. Image size: 50 nm×50 nm for a-g, 20 nm×20 nm for h.

Given that the surface free energy of Ni is higher than Au at high enough temperature Ni diffuses towards the bulk of Au. Since Ni has a smaller atomic radius than Au, subsurface Ni should introduce expansive strain in the surface. The effect of that strain on the local Au electron density of states can be detected by STM. The subsurface substitution of Pd into Au, for example, produces characteristic three-lobed depressions in STM images.[43] To examine the atomic structure of the dilute Ni-Au alloys in greater detail, we therefore acquired additional high-resolution STM images. Figure 3a shows a large-area STM image of the Au(111) surface after deposition of ~0.02 ML Ni at 550 K, revealing many depressions. An atomic resolution image of

a single depression is reproduced in the inset, along with a line-scan profile (Figure 3b) showing a depth of approximately 22 pm which is close to the reported one of ~30 pm.[32] A larger area atomic-resolution STM image was recorded (Figure 3c) by operating at 5 K to increase resolution and reduce thermal drift. A zoom of two Ni atoms is reproduced in Figure 3d. The features appear in STM images as slightly depressed Au atoms, small protrusions of single-atom diameter in perfect registry with the overlaying Au(111)-(1×1) lattice. A line-scan of one of the atoms (Figure 3d) showed a depth of approximately 6 pm, much smaller than that imaged Figure 3b (~22 pm). Comparison of the high-resolution and low-resolution STM images reveals that each such small protrusion corresponds to one depression observed at 80 K. The different apparent size of the atoms in Figure 3b and d is attributed to the different imaging parameters and different STM tips.

To interpret these observations, we used DFT to simulate STM images of Ni alloyed into the first and second surface layers of the unreconstructed fcc Au(111) supercell. We used the Tersoff-Hamann model which states that the tunneling current between the surface and the STM tip is proportional to the local density of states (LDOS) integrated over the bias range to the Fermi level.[44] The STM tip was approximated as an infinitesimal point source and the bias was set to 0.1 eV above the Fermi level. Integration over the LDOS was set to be constant by varying the distance of the point tip above the surface; a constant value for LDOS integration corresponds to constant current density (1×10^{-4} eV·Å^{-3}). We mapped the tip height above the surface onto a 2D grayscale plot, giving the images shown in Figure 3e and f. The scanning conditions used in the simulation of Figure 3e and f are similar to those used to record the STM images in Figure 3c and d. In Figure 3e, Ni appears as slightly depressed atom, a single small protrusion in the plane of the Au(111)-(1×1) structure, in agreement with our experimental

images. These findings suggest that predominately Ni-Au SAAs are generated from the deposition of Ni onto Au(111) above 500 K and that each depression imaged in STM corresponds to a single substitutional Ni atom in the *first surface layer*. On the contrary, the DFT simulated images show that regardless of STM imaging parameters *subsurface* Ni always produces triangular features (*e.g.* Figure 3f), which are not generally observed in the experimental STM images. Even so, the subsurface Ni should not be excluded as it is more favorable energetically than the surface Ni (~0.41 eV, according to our DFT calculations). While their occurrence is rare we cannot rule out the formation of some larger ensembles at the lower temperatures ~500 K, however, deposition ≥ 550 K produces predominately Ni-Au SAAs.

Overall, our results demonstrate that Ni-Au SAAs can be produced reliably on Au(111) by tuning the substrate temperature. The minimum temperature to form island-free SAA surfaces is ~550 K. This low temperature boundary will shift if the Ni flux is adjusted, as the kinetics of alloying would change. Further increases in temperature reduce the population of SAAs by driving surface Ni into the bulk. The Ni coverage of the alloys can be checked by analyzing the concentrations of depressions in the STM images, which exhibit a strong dependence on the substrate temperature during alloying and the amount of deposited Ni. Around half the deposited Ni atoms appear in the surface layer in the form of SAAs at 550 K, 600 K and 650 K when 0.004 ML Ni was deposited (Figure 1f-h) and at 550 K and 600 K when 0.02 ML Ni was deposited (Figure 2e-f). The maximum coverage of Ni-Au SAAs we observed was ~0.04 ML (*e.g.* Figure 2h) and alloying more Ni into the surface altered the herringbone reconstruction of Au(111).

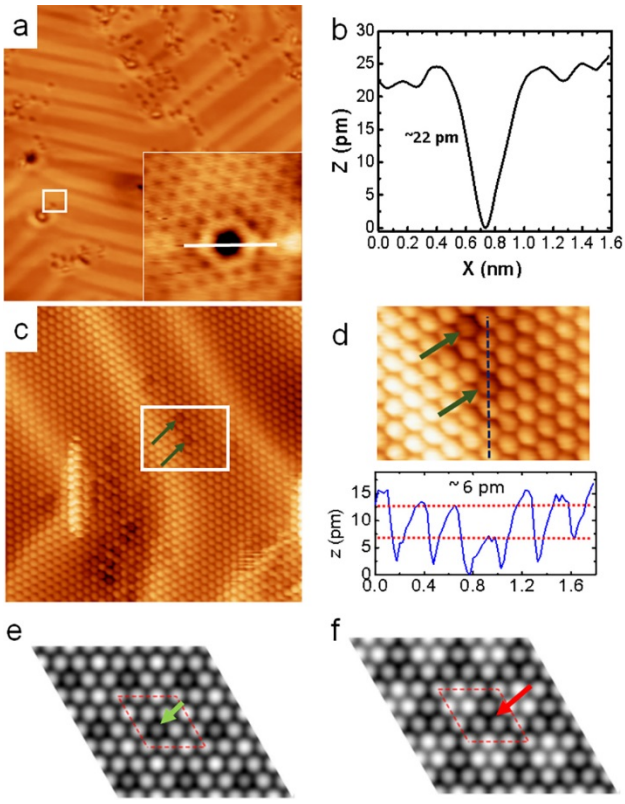

Figure 3. (a) STM image of a Au(111) surface after deposition of ~0.02 ML of Ni at 550 K (20 nm×20 nm, 100 mV, 2.7 nA, 80 K). Insert (2.7 nm×2.7 nm): atomic-resolution STM image of the highlighted depression. White line indicates the direction of the line scan profile reproduced in (b). (c) Atomic resolution STM image of a Au(111) surface after deposition of 0.02 ML of Ni at 550 K (10 nm×10 nm, 10 mV, 2.7 nA, 5 K). (d) Zoom of the area highlighted in (c) (2.5 nm×2.0 nm, 10 mV, 2.7 nA, 5 K) with the line scan of a single Ni atom substitution. (e, f) DFT-simulated STM image (charge density: 5×10^{-4} e·Å^{-3}) of a Ni atom surface substitution (e) and subsurface substitution (f). Green arrows highlight Ni-Au SAAs, and the red arrow points out the 3-fold hollow site on top of the subsurface Ni.

We used CO to probe the binding strength of Ni-Au SAAs. CO has a weak interaction with Au but bonds strongly to Ni, making it an ideal probe molecule.[45-46] The reactivity of Ni

stems from its partially filled d-band close to the Fermi level. Single-atom substitution of Ni into the Au surface creates expansive strain that would be expected to shift the Ni d-band even closer to the Fermi level, potentially making Ni/Au(111) even more reactive than Ni(111).[47-48] Strong interactions between CO and Ni-Au SAAs are therefore expected. Figure 4a reproduces an STM image of Au(111) exposed to ~0.05 L CO. Due to their weak interaction with Au, CO molecules are mobile even at 5 K under the influence of the tip, often producing blurry STM images. Annealing to 100 K completely desorbs the CO molecules, leaving only the clean Au(111) herringbone reconstruction (Figure 4b). In rare cases, a CO monomer from background adsorption appears as a bright protrusion surrounded by a dark halo (Figure 4c, white arrows).[49] To study the interaction of CO with Ni-Au SAAs, we deposited ~0.02 ML Ni on Au(111) at 550 K to create a SAA. We then examined the substrate after exposure to ~0.05 L CO (Figure 4d), and after annealing to 100 K (Figure 4e) and 220 K (Figure 4f). Before annealing, we again observe a 'blurry' image of the system due to the presence of CO. Despite the presence of Ni, this is expected because the surface remains predominantly Au. In contrast to the bare Au(111) surface however, a significant population of CO remains on the surface after a 100 K anneal (see blue arrows). The location of the remaining CO molecules correspond to the locations of Ni-Au SAAs prior to CO exposure, indicating that the CO is, as expected, strongly interacting with the Ni-Au SAAs. Although CO molecules appear as depressions in the large-area images, small-area images (*e.g.* Figure 4e inset) reveal that each depression contains a small protrusion in the center. The Ni-Au SAA interaction is sufficiently strong such that CO remains even after annealing to 220 K (Figure 4f, see blue arrows). These findings suggest that alloying dilute Ni atoms into a Au(111) surface significantly increases the reactivity of the substrate.

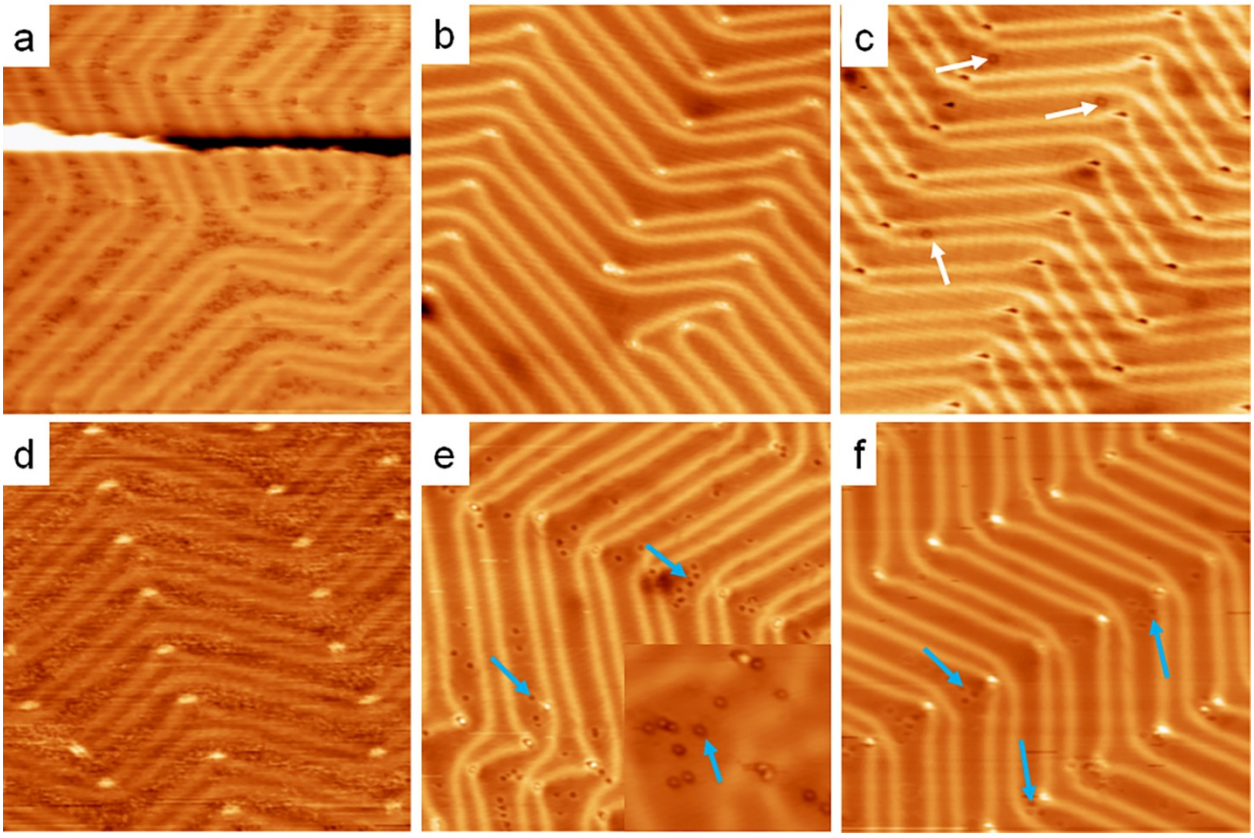

Figure 4. (a,b,c) STM images of clean Au(111) surfaces after exposure to ~0.05 L CO (a) followed by a 100 K anneal (b, c). (d,e,f) STM images of a Ni/Au(111) surface (~0.02 ML of Ni deposition at 550 K) after exposure to 0.05 L CO (d) followed by 100 K (e) and 220 K (f) anneals. The inset in (e) enlarges a region showing CO adsorbed at Ni-Au SAAs. Imaging conditions: 100 mV, 2.0 nA, 5 K. Image sizes: 50 nm×50 nm, and the size of the insert of (e): 10 nm × 10 nm. White and blue arrows highlight CO molecules adsorbed on Au(111) and Ni-Au SAAs, respectively.

Table 1 shows the calculated adsorption energies (E_{ads}) of CO on Ni(111), Au(111), on top of Ni in Ni-Au SAA, and on top of subsurface Ni embedded in Au(111). In all cases, we report CO on atop sites (most exothermic binding configuration) where the coverage of CO is

1/9 ML. While CO has a small adsorption energy on bare Au(111), the adsorption energy on top of Ni in the first layer of Au(111) is very large (-1.79 eV), even comparable with the adsorption energy of CO on Ni(111) (-1.75 eV). This calculation confirms our experimental conclusion that Ni-Au SAAs significantly increase the activity of Au(111). Note that the interaction of CO with subsurface Ni in Au(111) is very weak (-0.42 eV), similar to that of CO on Au(111), in agreement with previous reports.[50] Alloying Ni into the sub-surface would therefore have little impact on the activity of CO.

surface	**adsorption Site**	**E_{ads} (eV)**
Ni(111)	Ni_{atop}	-1.75
Au(111)	Au_{atop}	-0.46
Ni-Au(111) SAA	Ni_{atop}	-1.79
Ni-Au(111) subsurface Ni	Au_{atop}	-0.42

Table 1 DFT-calculated adsorption energies (E_{ads}) of CO on Ni(111), Au(111), on top of Ni in Ni-Au SAA, and on top of subsurface Ni in Au(111). The adsorption energy of CO is defined as the difference between the total energy of the CO adsorbed slab and the sum of the total energies of the clean slab and gas phase CO.

4. Conclusion

In conclusion, we have demonstrated a range of preparations of Ni-Au SAAs in the surface of Au(111) by tuning the substrate temperature during Ni physical vapor deposition. By raising the substrate temperature above 550 K during deposition, predominantly SAA Ni-Au surfaces can be produced. The SAA formation is the result of higher Ni adatom diffusion and substitution rates at elevated temperatures, yielding both increased surface substitution and

degradation of the Ni islands formed at lower temperature. Combined STM analysis and DFT image simulation reveal that the depressions observed at high temperature reflect isolated single Ni atoms alloyed into the top layer of Au(111). Finally, we examined the adsorption and desorption of CO onto the Ni-Au SAAs, finding that there is a significant enhancement of the molecule-substrate interaction. Mostly interestingly our DFT calculations reveal that single atoms on Ni in Au bind CO as strongly as Ni(111). Therefore, Ni-Au SAAs may significantly increase the surface activity of Au(111) and future work is aimed at interrogating the surface reactivity of this alloy using temperature programmed reactions.

Acknowledgment. We gratefully acknowledge support by Integrated Mesoscale Architectures for Sustainable Catalysis, an Energy Frontier Research Center funded by the U.S. Department of Energy, Office of Science, Basic Energy Sciences under Award No. DESC0012573. A.M.'s work is supported by the European Research Council under the European Union's Seventh Framework Programme (FP/2007-2013)/ERC Grant Agreement No. 616121 (Het-eroIce project) and the Royal Society through a Wolfson Research merit Award. M.D. is funded by the Engineering and Physical Sciences Research Council UK as part of a Doctoral Training Grant. The authors acknowledge the use of the UCL High Performance Computing Facilities (Legion@UCL and Grace@UCL), and associated support services, in the completion of the computational part of this work.

References

1. Janssens, T. W.; Clausen, B.; Hvolbæk, B.; Falsig, H.; Christensen, C.; Bligaard, T.; Nørskov, J., Insights into the Reactivity of Supported Au Nanoparticles: Combining Theory and Experiments. *Top. Catal.* **2007**, *44*, 15-26.

2. Pan, M.; Brush, A. J.; Pozun, Z. D.; Ham, H. C.; Yu, W.-Y.; Henkelman, G.; Hwang, G. S.; Mullins, C. B., Model Studies of Heterogeneous Catalytic Hydrogenation Reactions with Gold. *Chem. Soc. Rev.* **2013**, *42*, 5002-5013.

3. Liu, X.; Madix, R. J.; Friend, C. M., Unraveling Molecular Transformations on Surfaces: A Critical Comparison of Oxidation Reactions on Coinage Metals. *Chem. Soc. Rev.* **2008**, *37*, 2243-2261.

4. Min, B. K.; Friend, C. M., Heterogeneous Gold-Based Catalysis for Green Chemistry: Low-Temperature CO Oxidation and Propene Oxidation. *Chem. Rev.* **2007**, *107*, 2709-2724.

5. Liu, X.; Xu, B.; Haubrich, J.; Madix, R. J.; Friend, C. M., Surface-Mediated Self-Coupling of Ethanol on Gold. *J. Am. Chem. Soc.* **2009**, *131*, 5757-5759.

6. Wittstock, A.; Zielasek, V.; Biener, J.; Friend, C. M.; Bäumer, M., Nanoporous Gold Catalysts for Selective Gas-Phase Oxidative Coupling of Methanol at Low Temperature. *Science* **2010**, *327*, 319-322.

7. Xu, B.; Siler, C. G. F.; Madix, R. J.; Friend, C. M., Ag/Au Mixed Sites Promote Oxidative Coupling of Methanol on the Alloy Surface. *Chem. Eur. J.* **2014**, *20*, 4646-4652.

8. Claus, P., Heterogeneously Catalysed Hydrogenation Using Gold Catalysts. *Appl. Catal. A-Gen* **2005**, *291*, 222-229.

9. Mavrikakis, M.; Stoltze, P.; Nørskov, J. K., Making Gold Less Noble. *Catal. Lett.* **2000**, *64*, 101-106.

10. Hammer, B.; Norskov, J. K., Why Gold Is the Noblest of All the Metals. *Nature* **1995**, *376*, 238-240.

11. Cullen, W. G.; First, P. N., Island Shapes and Intermixing for Submonolayer Nickel on Au(111). *Surf. Sci.* **1999**, *420*, 53-64.

12. Trant, A. G.; Jones, T. E.; Gustafson, J.; Noakes, T. C. Q.; Bailey, P.; Baddeley, C. J., Alloy Formation in the Au{1 1 1}/Ni System – an Investigation with Scanning Tunnelling Microscopy and Medium Energy Ion Scattering. *Surf. Sci.* **2009**, *603*, 571-579.

13. Skriver, H. L.; Rosengaard, N. M., Surface Energy and Work Function of Elemental Metals. *Phys. Rev. B* **1992**, *46*, 7157-7168.

14. Christensen, A.; Ruban, A. V.; Stoltze, P.; Jacobsen, K. W.; Skriver, H. L.; Nørskov, J. K.; Besenbacher, F., Phase Diagrams for Surface Alloys. *Phys. Rev. B* **1997**, *56*, 5822-5834.

15. Larsen, J. H.; Chorkendorff, I., From Fundamental Studies of Reactivity on Single Crystals to the Design of Catalysts. *Surf. Sci. Rep.* **1999**, *35*, 163-222.

16. Dry, M. E., The Fischer–Tropsch Process: 1950–2000. *Catal. Today* **2002**, *71*, 227-241.

17. Rozovskii, A.; Lin, G., Fundamentals of Methanol Synthesis and Decomposition. *Top. Catal.* **2003**, *22*, 137-150.

18. Killelea, D. R.; Campbell, V. L.; Shuman, N. S.; Smith, R. R.; Utz, A. L., Surface Temperature Dependence of Methane Activation on Ni(111). *J. Phys. Chem. C* **2009**, *113*, 20618-20622.

19. Pei, G. X.; Liu, X. Y.; Wang, A.; Lee, A. F.; Isaacs, M. A.; Li, L.; Pan, X.; Yang, X.; Wang, X.; Tai, Z., et al., Ag Alloyed Pd Single-Atom Catalysts for Efficient Selective Hydrogenation of Acetylene to Ethylene in Excess Ethylene. *ACS Catal.* **2015**, *5*, 3717-3725.

20. Pei, G. X.; Liu, X. Y.; Wang, A.; Li, L.; Huang, Y.; Zhang, T.; Lee, J. W.; Jang, B. W. L.; Mou, C. Y., Promotional Effect of Pd Single Atoms on Au Nanoparticles Supported on Silica for the Selective Hydrogenation of Acetylene in Excess Ethylene. *New J. Chem.* **2014**, *38*, 2043-2051.

21. Aich, P.; Wei, H.; Basan, B.; Kropf, A. J.; Schweitzer, N. M.; Marshall, C. L.; Miller, J. T.; Meyer, R., Single-Atom Alloy Pd–Ag Catalyst for Selective Hydrogenation of Acrolein. *J. Phys. Chem. C* **2015**, *119*, 18140-18148.

22. McCue, A. J.; Gibson, A.; Anderson, J. A., Palladium Assisted Copper/Alumina Catalysts for the Selective Hydrogenation of Propyne, Propadiene and Propene Mixed Feeds. *Chem. Eng. J.* **2016**, *285*, 384-391.

23. Cao, X.; Ji, Y.; Luo, Y., Dehydrogenation of Propane to Propylene by a Pd/Cu Single-Atom Catalyst: Insight from First-Principles Calculations. *J. Phys. Chem. C* **2015**, *119*, 1016-1023.

24. Zhang, H.; Kawashima, K.; Okumura, M.; Toshima, N., Colloidal Au Single-Atom Catalysts Embedded on Pd Nanoclusters. *J. Mater. Chem. A* **2014**, *2*, 13498-13508.

25. Cheng, X.; Zhao, Y.; Li, F.; Liu, Y., Catalytic Mechanisms of Au_{11} and $Au_{11-n}Pt_n$ (n=1–2) Clusters: A DFT Investigation on the Oxidation of CO by O_2.. *J. Mol. Model.* **2015**, *21*, 1-11.

26. Yao, Y.; Goodman, D. W., New Insights into Structure-Activity Relationships for Propane Hydrogenolysis over Ni-Cu Bimetallic Catalysts. *RSC Adv.* **2015**, *5*, 43547-43551.

27. Zhang, L.; Wang, A.; Miller, J. T.; Liu, X.; Yang, X.; Wang, W.; Li, L.; Huang, Y.; Mou, C.-Y.; Zhang, T., Efficient and Durable Au Alloyed Pd Single-Atom Catalyst for the Ullmann Reaction of Aryl Chlorides in Water. *ACS Catal.* **2014**, *4*, 1546-1553.

28. Kyriakou, G.; Boucher, M. B.; Jewell, A. D.; Lewis, E. A.; Lawton, T. J.; Baber, A. E.; Tierney, H. L.; Flytzani-Stephanopoulos, M.; Sykes, E. C. H., Isolated Metal Atom Geometries as a Strategy for Selective Heterogeneous Hydrogenations. *Science* **2012**, *335*, 1209-1212.

29. Lucci, F. R.; Liu, J.; Marcinkowski, M. D.; Yang, M.; Allard, L. F.; Flytzani-Stephanopoulos, M.; Sykes, E. C. H., Selective Hydrogenation of 1,3-Butadiene on Platinum-Copper Alloys at the Single-Atom Limit. *Nat. Commun.* **2015**, *6*. 8550.

30. Besenbacher, F.; Chorkendorff, I.; Clausen, B. S.; Hammer, B.; Molenbroek, A. M.; Nørskov, J. K.; Stensgaard, I., Design of a Surface Alloy Catalyst for Steam Reforming. *Science* **1998**, *279*, 1913-1915.

31. Pleth Nielsen, L.; Besenbacher, F.; Stensgaard, I.; Laegsgaard, E.; Engdahl, C.; Stoltze, P.; Jacobsen, K. W.; Nørskov, J. K., Initial Growth of Au on Ni(110): Surface Alloying of Immiscible Metals. *Phys. Rev. Lett.* **1993**, *71*, 754-757.

32. Meyer, J. A.; Baikie, I. D.; Kopatzki, E.; Behm, R. J., Preferential Island Nucleation at the Elbows of the Au(111) Herringbone Reconstruction through Place Exchange. *Surf. Sci.* **1996**, *365*, L647-L651.

33. Chambliss, D. D.; Wilson, R. J.; Chiang, S., Ordered Nucleation of Ni and Au Islands on Au(111) Studied by Scanning Tunneling Microscopy. *J. Vac. Sci. Technol. B* **1991**, *9*, 933-937.

34. Therrien, A. J.; Pronschinske, A.; Murphy, C. J.; Lewis, E. A.; Liriano, M. L.; Marcinkowski, M. D.; Sykes, E. C. H., Effects in Physisorbed Molecular Hydrogen on Ni/Au(111). *Phys. Rev. B* **2015**, *92*, 161407.

35. Kresse, G.; Hafner, J., *Ab* Initio Molecular Dynamics for Liquid Metals. *Phys. Rev. B* **1993**, *47*, 558-561.

36. Kresse, G.; Furthmüller, J., Efficient Iterative Schemes for *Ab* Initio Total-Energy Calculations Using a Plane-Wave Basis Set. *Phys. Rev. B* **1996**, *54*, 11169-11186.

37. Klimeš, J.; Bowler, D. R.; Michaelides, A., Chemical Accuracy for the van der Waals Density Functional. *J. Phys.: Condens. Matter* **2010**, *22*, 022201.

38. Klimeš, J.; Bowler, D. R.; Michaelides, A., Van der Waals Density Functionals Applied to Solids. *Phys. Rev. B* **2011**, *83*, 195131.

39. Dion, M.; Rydberg, H.; Schröder, E.; Langreth, D. C.; Lundqvist, B. I., Van der Waals Density Functional for General Geometries. *Phys. Rev. Lett.* **2004**, *92*, 246401.

40. Wöll, C.; Chiang, S.; Wilson, R. J.; Lippel, P. H., Determination of Atom Positions at Stacking-Fault Dislocations on Au(111) by Scanning Tunneling Microscopy. *Phys. Rev. B* **1989**, *39*, 7988-7991.

41. Barth, J. V.; Brune, H.; Ertl, G.; Behm, R. J., Scanning Tunneling Microscopy Observations on the Reconstructed Au(111) Surface: Atomic Structure, Long-Range

Superstructure, Rotational Domains, and Surface Defects. *Phys. Rev. B* **1990**, *42*, 9307-9318.

42. Howard, A.; Mitchell, C. E. J.; Egdell, R. G., Real Time STM Observation of Ostwald Ripening of Pd Nanoparticles on TiO_2(110) at Elevated Temperature. *Surf. Sci.* **2002**, *515*, L504-L508.

43. Baber, A. E.; Tierney, H. L.; Sykes, E. C. H., Atomic-Scale Geometry and Electronic Structure of Catalytically Important Pd/Au Alloys. *ACS Nano* **2010**, *4*, 1637-1645.

44. Tersoff, J.; Hamann, D. R., Theory of the Scanning Tunneling Microscope. *Phys. Rev. B* **1985**, *31*, 805-813.

45. Hammer, B.; Morikawa, Y.; Nørskov, J. K., CO Chemisorption at Metal Surfaces and Overlayers. *Phys. Rev. Lett.* **1996**, *76*, 2141-2144.

46. Miller, J. B.; Siddiqui, H. R.; Gates, S. M.; Russell, J. N.; Yates, J. T.; Tully, J. C.; Cardillo, M. J., Extraction of Kinetic Parameters in Temperature Programmed Desorption: A Comparison of Methods. *J. Chem. Phys.* **1987**, *87*, 6725-6732.

47. Ruban, A.; Hammer, B.; Stoltze, P.; Skriver, H. L.; Nørskov, J. K., Surface Electronic Structure and Reactivity of Transition and Noble Metals. *J. Mol. Catal. A: Chem.* **1997**, *115*, 421-429.

48. Pedersen, M. Ø.; Helveg, S.; Ruban, A.; Stensgaard, I.; Lægsgaard, E.; Nørskov, J. K.; Besenbacher, F., How a Gold Substrate Can Increase the Reactivity of a Pt Overlayer. *Surf. Sci.* **1999**, *426*, 395-409.

49. Maksymovych, P.; Yates Jr, J. T., Unexpected Spontaneous Formation of CO Clusters on the Au(1 1 1) Surface. *Chem. Phys. Lett.* **2006**, *421*, 473-477.

50. Tenney, S. A.; He, W.; Roberts, C. C.; Ratliff, J. S.; Shah, S. I.; Shafai, G. S.; Turkowski, V.; Rahman, T. S.; Chen, D. A., CO-Induced Diffusion of Ni Atoms to the Surface of Ni–Au Clusters on TiO_2(110). *J. Phys. Chem. C* **2011**, *115*, 11112-11123.

TOC Graphic